

Influence of Initial Conditions on Propagation, Growth and Decay of Saturation Overshoot

R. Steinle¹ · R. Hilfer¹

Received: 24 November 2014 / Accepted: 5 November 2015 / Published online: 13 January 2016
© Springer Science+Business Media Dordrecht 2016

Abstract A sequence of drainage and imbibition shocks within the traditional theory of two-phase immiscible displacement can give rise to shallow non-monotone saturation profiles as shown in Hilfer and Steinle (Eur Phys J Spec Top 223:2323, 2014). This phenomenon depends sensitively on model parameters and initial conditions. The dependence of saturation overshoot on initial conditions is investigated more systematically in this article. The results allow to determine regions in the parameter space for the observation of saturation overshoot and to explore limitations of the underlying idealized hysteresis model. Numerical solutions of the nonlinear partial differential equations of motion reveal a strong dependence of the overshoot phenomenon on the boundary and initial conditions. Overshoot solutions with experimentally detectable height are shown to exist numerically. Extensive parameter studies reveal different classes of initial conditions for which the width of the overshoot region can decrease, increase or remain constant.

Keywords Saturation overshoot · Dependence on initial conditions · Two-phase flow · Hysteresis

1 Introduction

Analytical approximations and numerical solutions have recently predicted the existence of a class of travelling and non-travelling saturation overshoot profiles within the standard traditional two-phase flow equations for immiscible displacement in porous media (Hilfer and Steinle 2014). Displacing a lighter fluid with a heavier fluid is expected to cause instabilities, preferential flow paths and saturation overshoot (Hilfer and Steinle 2014; Xiong 2014).

Mathematical arguments, however, seem to exclude non-monotone profiles within the Richards approximation to the standard two-phase flow equations (Alt and Luckhaus 1983;

✉ R. Hilfer
hilfer@icp.uni-stuttgart.de

¹ Institute for Computational Physics (ICP), Universität Stuttgart, Allmandring 3, 70569 Stuttgart, Germany

Alt et al. 1984; Otto 1996; Egorov et al. 2003). Accordingly, “there is a wide spread belief (mainly as a result of anomalous experimental results) that the standard multiphase model is incomplete” (di Carlo 2013, p. 4541). If the standard multiphase model were indeed incomplete (see Hilfer 2006a, b), then this would imply “the necessity of extensions to the multiphase flow equations to describe the unstable flow” (di Carlo 2013, p. 4531). One extension proposes various additional terms in the Richards equation to accommodate saturation overshoot (Eliassi and Glass 2002). Relaxation terms are proposed in Egorov et al. (2003) to produce unstable flows and fingering. Extensions from static to so-called dynamic capillarity were investigated in Beliaev and Hassanizadeh (2001), Duijn et al. (2007, 2013) and Rätz et al. (2014). Multiphase flow equations based on a phase field approach were suggested in Cueto-Felgueroso and Juanes (2008, 2009).

Despite the widespread belief that the standard multiphase model is incomplete, recent investigations have reported solutions of the standard two-phase flow equations exhibiting saturation overshoot (Hilfer and Steinle 2014). Evidence for travelling and non-travelling overshoot profiles, albeit shallow ones, was presented in Hilfer and Steinle (2014) on the basis of analytical considerations and numerical simulations. It was found that the existence of saturation overshoot depended sensitively on the initial and boundary conditions.

2 Problem and Objective

Given that the computations reported in Hilfer and Steinle (2014) have found travelling non-monotone saturation profile with a very small overshoot height $\Delta S = 0.0554$, the problem arises how to observe such small overshoots in experiment. Lest one has to wait for precision experiments to test this prediction, the present article explores the parameter space in search for larger overshoot. Occurrence of overshoot was found in Hilfer and Steinle (2014) to depend sensitively on the initial conditions. Roughly two-dozen parameters specifying the constitutive assumptions enter into the mathematical model. It is not possible to carry out a complete, exhaustive or even systematic study of the full parameter space due to its high dimensionality. As a result, the primary problem here is to elucidate first the known sensitive dependence on the parameters in the initial data. More systematic explorations of the multidimensional parameter space are only useful, if the sensitive dependence on initial conditions has been understood and can be reliably predicted.

These problems motivate the twofold objective of this article. The first objective is to find a set of parameters allowing for a sufficiently high saturation overshoot to be unambiguously observable in experiment. The second objective is to fix these parameters for a sufficiently high overshoot and explore the parameter space of the initial conditions systematically. This will help to understand and identify the regions where overshoot is possible, at least within a low-dimensional subspace of all admissible initial conditions.

3 Mathematical Model

The mathematical model describes two-phase immiscible displacement in a narrow column oriented parallel to the direction of gravity. The equations of motion govern the unknown saturation field $S(z, t)$ of a wetting phase, called water \mathbb{W} . Here $0 \leq z < \infty$ is the coordinate along the vertical one-dimensional column, and $t \geq 0$ denotes time. The nonlinear partial differential equation for $S(z, t)$ reads

$$\begin{aligned} \phi \frac{\partial S}{\partial t} + \mathcal{E}(S) Q \frac{\partial}{\partial z} \left[f_{\text{im}}(S) - D_{\text{im}}(S) \frac{\partial S}{\partial z} \right] \\ + [1 - \mathcal{E}(S)] Q \frac{\partial}{\partial z} \left[f_{\text{dr}}(S) - D_{\text{dr}}(S) \frac{\partial S}{\partial z} \right] = 0 \end{aligned} \tag{1}$$

where ϕ is the porosity of the medium and Q denotes the total volume flux of (wetting and non-wetting) fluids. The projector function $\mathcal{E} : \mathbb{R} \rightarrow \{0, 1\}$

$$\mathcal{E}(S) = \lim_{\varepsilon \rightarrow 0} \Theta \left[\frac{\partial S}{\partial t}(z, t - \varepsilon) \right], \tag{2}$$

with

$$\Theta(x) = \begin{cases} 1, & x > 0 \\ 0, & x \leq 0 \end{cases} \tag{3}$$

switches between imbibition and drainage. The nonlinear constitutive parameter functions are the fractional flow functions

$$f_i(S) = \frac{1 + k_{\mathbb{W}i}^r(S) \frac{\varrho_{\mathbb{W}gk}}{Q\mu_{\mathbb{O}}} \left(1 - \frac{\varrho_{\mathbb{O}}}{\varrho_{\mathbb{W}}}\right)}{1 + \frac{\mu_{\mathbb{W}}}{\mu_{\mathbb{O}}} \frac{k_{\mathbb{O}i}^r(S)}{k_{\mathbb{W}i}^r(S)}} \tag{4}$$

for drainage ($i = \text{dr}$) and imbibition ($i = \text{im}$), and the capillary flux functions

$$D_i(S) = - \frac{k_{\mathbb{W}i}^r(S) \frac{k}{\mu_{\mathbb{W}}Q} \frac{dP_{Ci}(S)}{dS}}{1 + \frac{\mu_{\mathbb{O}}}{\mu_{\mathbb{W}}} \frac{k_{\mathbb{W}i}^r(S)}{k_{\mathbb{O}i}^r(S)}} \tag{5}$$

with $i \in \{\text{im}, \text{dr}\}$. Here $\varrho_{\mathbb{W}}, \varrho_{\mathbb{O}}$ denote the densities and $\mu_{\mathbb{W}}, \mu_{\mathbb{O}}$ the viscosities of the wetting phase \mathbb{W} (called water) and the non-wetting phase \mathbb{O} (called oil). The acceleration of gravity is g , and the absolute permeability of the porous medium is k . The relative permeability functions $k_{\mathbb{W}i}^r, k_{\mathbb{O}i}^r$ are assumed to be algebraic functions

$$k_{\mathbb{W}i}^r(S_{ei}) = K_{\mathbb{W}i}^e S_{ei}^{\alpha_i} \tag{6a}$$

$$k_{\mathbb{O}i}^r(S_{ei}) = K_{\mathbb{O}i}^e (1 - S_{ei})^{\beta_i} \tag{6b}$$

of the effective saturation

$$S_{ei} = \frac{S - S_{\mathbb{W}i}^i}{1 - S_{\mathbb{O}r}^i - S_{\mathbb{W}i}^i} \tag{7}$$

with $i \in \{\text{im}, \text{dr}\}$, where $K_{\mathbb{W}i}^e, K_{\mathbb{O}i}^e$ are the endpoints, α_i, β_i the exponents, $S_{\mathbb{W}i}^i$ is the irreducible wetting phase saturation and $S_{\mathbb{O}r}^i$ the irreducible non-wetting phase saturation. The capillary pressure functions are assumed to be of the form

$$P_{Ci}(S_{ei}) = P_{bi} \left(S_{ei}^{-1/\gamma_i} - 1 \right)^{1-\gamma_i} \tag{8}$$

as in Hilfer and Steinle (2014) with $i \in \{\text{im}, \text{dr}\}$.

Initially, the medium is assumed to be homogeneously saturated with non-wetting fluid. The initial condition for Eq. (1) is then a small constant wetting saturation

$$S(z, t = 0) = S^{\text{out}} \tag{9}$$

for all $z \geq 0$ throughout the porous medium. Constant Q and constant S^{in} are assumed for the boundary conditions at the left boundary. The boundary conditions at the inlet $z = 0$ and the outlet $z \rightarrow \infty$ then read

$$S(z = 0, t) = \begin{cases} S^{\text{P}}, & 0 \leq t < t^{\text{P}} \\ S^{\text{in}}, & t \geq t^{\text{P}} \end{cases} \tag{10a}$$

$$S(z \rightarrow \infty, t) = S^{\text{out}}, \quad t \geq 0 \tag{10b}$$

with $S^{\text{in}} = 0.35$ and $S^{\text{out}} = 0.01$ (see Table 1). Note that the boundary conditions at the inlet are time dependent and that they differ from experiments where the flux of the wetting phase and the pressure of the non-wetting phase are controlled at the boundary.

The initial value problem with time-dependent boundary values specified in Eq. (10) can be viewed also as an initial value problem with time-independent constant boundary values (S^{in} at the inlet and S^{out} at the outlet) if one uses $t = t^{\text{P}}$ instead of $t = 0$ as the initial instant. This point of view will often be used in the following discussions.

4 Fractional Flow Functions and Graphical Solutions

The initial and time-dependent boundary value problems specified in Eqs. (1)–(10) are closely related to the initial and boundary value problems studied in Hilfer and Steinle (2014). Following the analysis in Hilfer and Steinle (2014), graphical solutions can be found in the Buckley-Leverett limit ($D_i \rightarrow 0$).

For large $t^{\text{P}} \rightarrow \infty$, one expects to find a leading imbibition front followed by a drainage front. The two shock fronts are expected to be well separated and to move independently of each other with different speeds. For small $t^{\text{P}} \rightarrow 0$, one expects to find a single Buckley-Leverett imbibition shock.

For $0 < t^{\text{P}} < \infty$ and $t < t^{\text{P}}$, the solution is a single imbibition shock front that propagates into the medium as in conventional Buckley-Leverett theory. Below the saturation S^{Welge} of the Welge tangent construction, i.e. for $S^{\text{P}} \leq S^{\text{Welge}} \approx 0.6619$, the shock has height S^{P} . For $S^{\text{P}} > S^{\text{Welge}}$, the solution is a shock front with jump height S^{Welge} followed by a rarefaction wave. The rarefaction wave connects S^{Welge} and S^{P} . This is a typical imbibition front that moves with velocity $c_{\text{im}}(S^{\text{P}})$ or $c_{\text{im}}(S^{\text{Welge}})$ as predicted by the traditional Buckley-Leverett theory. In the following, $S^{\text{P}} \leq S^{\text{Welge}}$ will be assumed for simplicity.

For $0 < t^{\text{P}} < \infty$ and $t \geq t^{\text{P}}$, the inlet saturation is held constant at $S^{\text{in}} < S^{\text{P}}$. A trailing drainage front now follows the leading imbibition front resulting in a saturation overshoot. Whether or not the overshoot region persists for long times depends sensitively on the parameters ($S^{\text{P}}, t^{\text{P}}$) as discussed next.

The propagation velocities of the two shock fronts are obtained from the Rankine-Hugoniot condition as

$$c_{\text{im}}(S) =: \frac{f_{\text{im}}(S) - f_{\text{im}}(S^{\text{out}})}{S - S^{\text{out}}} \tag{11a}$$

Table 1 Parameter values, their symbols and units

Parameter	Symbol	Value	Units
Porosity	ϕ	0.38	–
Permeability	k	2×10^{-10}	m^2
Density \mathbb{W}	$\rho_{\mathbb{W}}$	1000	kg/m^3
Density \mathbb{O}	$\rho_{\mathbb{O}}$	1	kg/m^3
Viscosity \mathbb{W}	$\mu_{\mathbb{W}}$	0.001	Pa s
Viscosity \mathbb{O}	$\mu_{\mathbb{O}}$	0.0003	Pa s
Imb. exp. rel.p. \mathbb{W}	α_{im}	5	–
Imb. exp. rel.p. \mathbb{O}	α_{dr}	3	–
Dr. exp. rel.p. \mathbb{W}	β_{im}	3	–
Dr. exp. rel.p. \mathbb{O}	β_{dr}	5	–
End pnt. rel.p.	$K_{\mathbb{W}im}^e$	0.35	–
End pnt. rel.p.	$K_{\mathbb{O}im}^e$	1	–
End pnt. rel.p.	$K_{\mathbb{W}dr}^e$	0.35	–
End pnt. rel.p.	$K_{\mathbb{O}dr}^e$	0.75	–
Imb. exp. cap press.	γ_{im}	0.85	–
Dr. exp. cap press.	γ_{dr}	0.98	–
Imb. cap. press.	P_{bim}	1	Pa
Dr. cap. press.	P_{bdr}	1000	Pa
End pnt. sat.	$S_{\mathbb{W}i}^{im}$	0	–
End pnt. sat.	$S_{\mathbb{W}i}^{dr}$	0.07	–
End pnt. sat.	$S_{\mathbb{O}r}^{im}$	0.045	–
End pnt. sat.	$S_{\mathbb{O}r}^{dr}$	0.045	–
Outlet saturation	S^{out}	0.01	–
Inlet saturation	S^{in}	0.35	–
Welge sat.	S^{Welge}	0.6619	–
Total flux	Q	10^{-5}	m/s

for the imbibition front and

$$c_{dr}(S) =: \frac{f_{dr}(S) - f_{dr}(S^{in})}{S - S^{in}} \tag{11b}$$

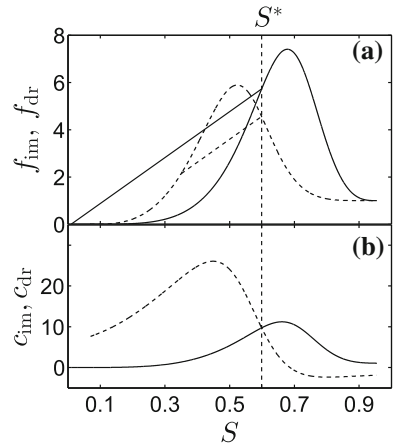
for the trailing drainage front. Equating the velocities results in the condition

$$c_{im}(S) = c_{dr}(S) \tag{12}$$

whose solution is the saturation $S = S^*$ at which both fronts move with the same speed. The solution depends on the inlet and outlet saturations $S^* = S^*(S^{in}, S^{out})$. Equation (12) can have no solution, one solution or several solutions (Hilfer and Steinle 2014).

The initial and time-dependent boundary value problems (1)–(10) are studied for the parameters given in Table 1. The resulting fractional flow functions from Eq. (4) are displayed in Fig. 1a. Figure 1b shows the shock front velocities from Eq. (11). The solution $S^*(S^{in}, S^{out})$

Fig. 1 **a** Fractional flow functions for imbibition (*solid*) and drainage (*dashed*) with parameters from Table 1. The two secants (*solid/dashed*) show the graphical construction of the travelling wave solution with $c_{im} = c_{dr} = 9.7$. Subfigure **b** shows the graphical solution of Eq. (12) as the intersection of the imbibition front velocity (*solid*) with the drainage front velocity (*dashed*)



of Eq. (12) is computed as $S^* = 0.5989$. The two secants in Fig. 1a represent the imbibition shock (solid secant) connecting $f_{im}(S^*)$ with $f_{im}(S^{out})$ and the drainage shock (dashed secant) connecting $f_{dr}(S^*)$ with $f_{dr}(S^{in})$. If these two secants are parallel and $S^{in} < S^* \leq S^{Wedge}$ then choosing $S^P = S^*$ in Eq. (10) produces an overshoot profile that propagates as a travelling wave as long as t^P is not too small. Figure 1b also shows that Eq. (12) has only one solution for the parameters given in Table 1.

In general, for $S^P \neq S^*$ in Eq. (10), a non-monotone overshoot profile propagates with distinct imbibition and drainage velocities $c_{dr}(S^P) \neq c_{im}(S^P)$. As a result, the width of the overshoot region changes linearly with time. For $c_{dr}(S^P) < c_{im}(S^P)$ the leading imbibition front is faster than the drainage front and the overshoot width broadens. For $c_{dr}(S^P) > c_{im}(S^P)$, the leading imbibition front is slower than the trailing drainage front and the width shrinks until a monotone saturation profile is left.

5 Discretization and Numerical Methods

The numerical solutions were computed using OpenFOAM (version 2.1.1), an open-source toolkit for computational fluid mechanics (<http://www.openfoam.com/>). To solve Eq. (1) required a new solver routine. It was derived from the solver `scalarTransportFoam`. A direct discretization of $\nabla_z \cdot f_i(S) \hat{=} \partial f_i(S) / \partial z$ in Eq. (1) using the `fvc::div`-operator has been implemented. A second discretization based on differentiating the flux function as $f'_i(S)^T \nabla_z S \hat{=} f'_i(S) \times \partial S / \partial z$ and using the `fvc::grad`-operator was also implemented to check the accuracy. Both discretizations gave identical results within numerical accuracy. All results reported here were obtained with the first direct discretization using the `fvc::div`-operator.

The second-order term had to be regularized by a maximum function replacing $D_i(S)$ with $\max_{S \in [0, 1]} \{D_i(S), 0.009m\}$ to avoid oscillations at the imbibition front. Such oscillations can arise from small values of the capillary flux functions $D_i(S)$.

The time derivative was discretized with an implicit Euler scheme. The gradient term was discretized with an explicit least-squares scheme, the divergence with an explicit Gauss cubic scheme, and the second-order term with an implicit Gauss linear corrected scheme.

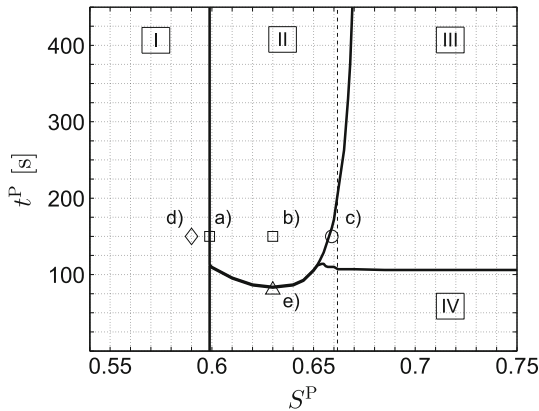


Fig. 2 (S^P, t^P)-parameter plane of initial data in Eq. (10a) divided into four regions I–IV with different asymptotic ($t \rightarrow \infty$)-behaviour of numerical solutions. In Region I and Region IV, the initial overshoot $S^P - S^{in}$ decays as $t \rightarrow \infty$, while in Region II and Region III the overshoot persists and the overshoot region broadens. On the *straight vertical* and *solid line* at $S^P = S^* = 0.5989$, the overshoot region has constant width and the profile is a travelling wave with constant velocity $c_{dr}(S^P) = c_{im}(S^P)$. In Region II, the plateau saturation for $t \rightarrow \infty$ equals the initial saturation S^P ; for Region III, the final saturation for $t \rightarrow \infty$ is smaller than S^P . The *vertical dashed line* marks the Welge saturation $S^{Welge} \approx 0.6619$

For more details on discretization, see (<http://www.openfoam.org/archive/2.1.1/docs/user/fvSchemes.php#x20-1070004.4>). Finally, the discretized system was solved with an incomplete Cholesky conjugate gradient solver (ICCG) supplied in OpenFOAM.

In all computations reported here, the spatial discretization is $\Delta z = 0.5$ mm and the temporal discretization is $\Delta t = 0.1$ s. It was checked that the results are within limits independent of this choice.

6 Numerical Solution

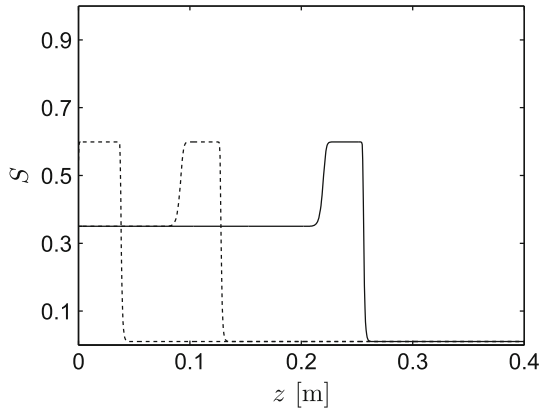
As specified in Sect. 2, the primary objective of this article is to explore systematically the parameter space of the initial data, because it was found in Hilfer and Steinle (2014) that the existence or non-existence of saturation overshoot depends sensitively on the initial condition. The parameter space of the initial condition Eq. (10a) is the (S^P, t^P)-plane.

More than two hundred numerical solutions with $S^P \in [0.55, 0.9]$, $t^P \in [50s, 4000 s]$ were performed and analysed manually, because an automated analysis was not practical with available resources. During these runs, all other parameters were kept fixed at their values given in Table 1. The results of these computations are summarized in Fig. 2. There are four different regions I–IV in Fig. 2. Region II and Region III indicate non-monotone solutions for $t \rightarrow \infty$, i.e. a saturation overshoot persists. Region IV and Region I correspond to parameters for which the initial overshoot decays into a monotone profile without overshoot.

A straight vertical line (solid) at $S^P = S^* = 0.5989$ separates Region I from the rest, because for $S^P < S^* = 0.5989$ one has $c_{dr}(S^P) > c_{im}(S^P)$ as seen in Fig. 1b. In Region I, the trailing drainage front catches up with leading imbibition front and annihilates the overshoot. Exactly on the straight vertical and solid line at $S^P = S^* = 0.5989$, the leading imbibition front and the trailing drainage front have the same velocity $c_{dr}(S^P) = c_{im}(S^P)$.

The boundaries between different regions in the (S^P, t^P)-plane are rough and approximate numerical estimates from numerous simulation runs. The straight vertical and solid line at $S^P = S^* = 0.5989$ separating Region I from the rest has the smallest numerical inaccuracy.

Fig. 3 Travelling saturation overshoot profile $S(z, t)$ solving Problem a) at times $t = 150$ s (dashed), $t = 500$ s (dashed) and $t = 1000$ s (solid). The profile travels with constant velocity $Qc_{im}(0.5989)/\phi = Qc_{dr}(0.5989)/\phi = 0.0255$ cm/s



On the right for $S^P > S^*$, the leading front is faster than the trailing one and the overshoot plateau broadens linearly with time except in Region IV. In Region IV, the initial width of the overshoot plateau is so small that the broadening of the trailing drainage front leads to its decay due to capillary effects. In Region II, the plateau broadens and the value of the plateau saturation stays constant at the initial saturation S^P for all t . In Region III, the plateau broadens, but the final saturation for $t \rightarrow \infty$ is smaller than S^P .

The following five initial and boundary problems are selected as representatives for the different classes of sensitive dependence on the initial data:

- Problem a): $(S^P, t^P) = (0.5989, 150 \text{ s})$
- Problem b): $(S^P, t^P) = (0.63, 150 \text{ s})$
- Problem c): $(S^P, t^P) = (0.659, 150 \text{ s})$
- Problem d): $(S^P, t^P) = (0.59, 150 \text{ s})$
- Problem e): $(S^P, t^P) = (0.63, 80 \text{ s})$.

The time-dependent solutions $S(z, t)$ to these five problems will now be plotted and discussed.

6.1 Problem a)

The numerical solution of Problem a) is illustrated in Fig. 3 at three different times $t = 150, 500, 1000$ s. It exhibits a pronounced overshoot of height $S^P - S^{in} = 0.5989 - 0.35 = 0.2489$ that can be detected in an experiment. The width of the overshoot region remains constant. Because $S^P = S^* = 0.5989$, it falls on the vertical straight line and the overshoot travels as a travelling wave solution with fixed constant velocity. The dimensionless value $c_{dr}(S^P) = c_{im}(S^P) = 9.7$ from the graphical solution in Fig. 1 agrees perfectly with the dimensional value $Qc_{im}(S^P)/\phi = 0.0255$ cm/s found from the numerical solution in Fig. 3.

The solution to Problem a) is shown also for all (z, t) in Fig. 4a as a three-dimensional surface plot. Figure 4a exhibits clearly the constant width of the overshoot region and the constant speed of the leading and trailing shocks.

6.2 Problem b)

The parameters of Problem b) fall into Region II, and its numerical solution is illustrated in Fig. 4b. Now $c_{dr}(S^P) < c_{im}(S^P)$, and the overshoot region broadens. Again, the front velocities are seen to be constant. Their numerical values measured directly from the numerical solutions, $Qc_{dr}(S^P)/\phi = 0.01369$ cm/s for drainage resp. $Qc_{im}(S^P)/\phi = 0.02834$ cm/s for

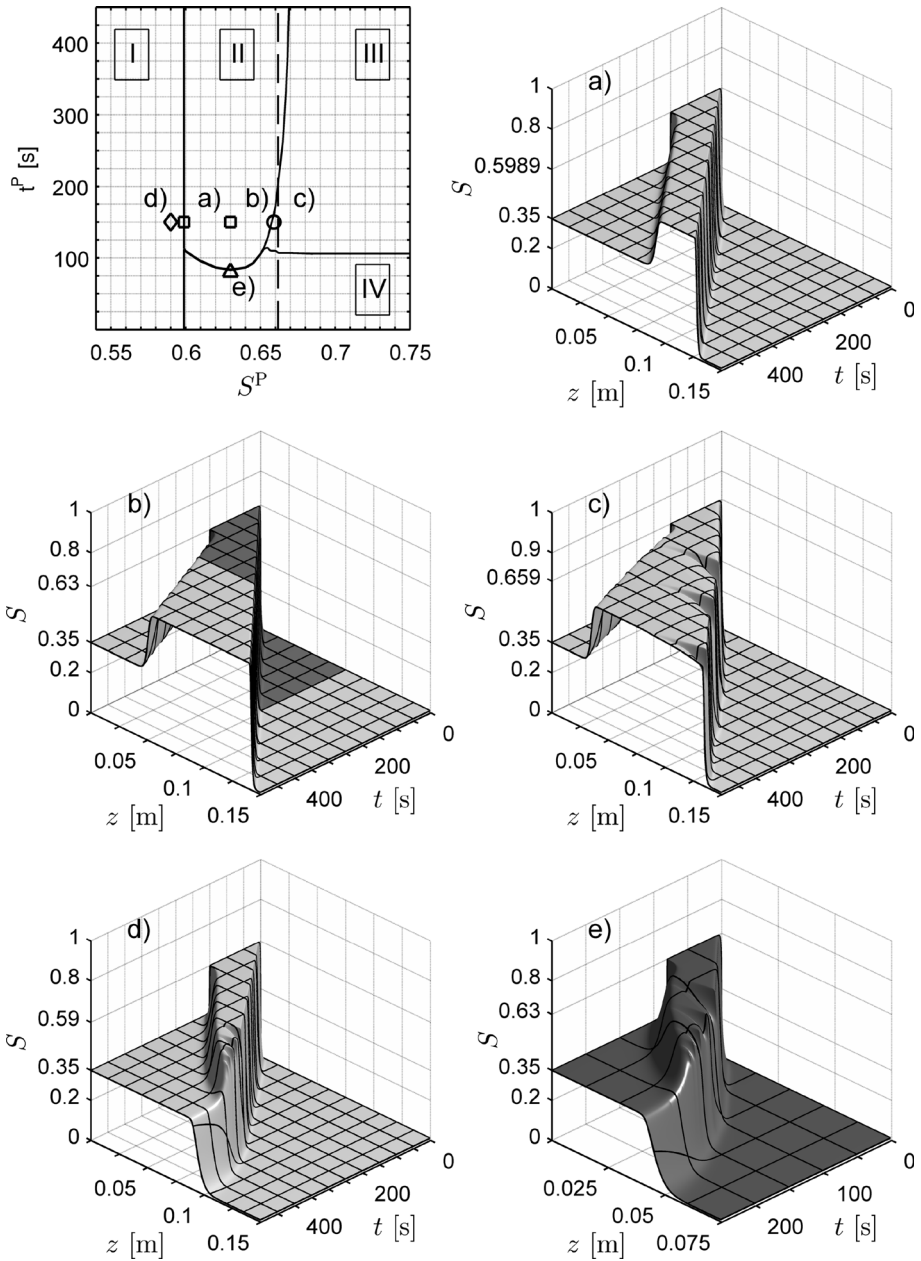


Fig. 4 Numerical solutions of Problems **a–e** representative for the domains I–IV in the (S^P, t^P) -plane from Fig. 2. Figure 2 is reproduced as the top left subfigure for convenience. Numerical solutions are visualized as three-dimensional surface plots with $\Delta z = 0.5$ mm and $\Delta t = 0.1$ s. To aid the eye gridlines with spacing 1.5 cm and 50 s are overlaid as *solid black lines*. Subfigure **a** shows travelling overshoot wave with overshoot saturation $S = S^* = 0.5989$. Subfigure **b** shows a non-monotone saturation profile with overshoot saturation $S = 0.63$ and increasing width. Subfigure **c** shows a non-monotone saturation profile with increasing width and decreasing height. Subfigure **d** shows the decay of an overshoot solution with decreasing width. Subfigure **e** shows an overshoot profile annihilated rapidly by capillary diffusion effects. Note the different scale of the t -axis in Subfigure **e**

imbibition, agree perfectly with the analytical predictions $c_{\text{dr}}(S^{\text{P}}) = 5.204$ and $c_{\text{im}}(S^{\text{P}}) = 10.77$. It is seen that the height of the plateau value stays fixed and constant at S^{P} for all t . In Fig. 4b, the region $0 \leq t \leq 250$ s is shaded darker to facilitate the comparison with Fig. 4e where only this region is plotted.

6.3 Problem c)

The numerical solution of problem c) is typical for initial and boundary value problems with parameters in Region III. The non-monotone profile exhibits fronts with unequal velocities. The overshoot saturation S^{P} is not stable and decreases, because it is typically larger than S^{Wolge} . The numerical solution of Problem c) for $t \rightarrow \infty$ and $t \gg t^{\text{P}}$ shows a non-travelling non-monotone saturation profile approaching a saturation $S \approx 0.631 < S^{\text{P}}$. For $t > t^{\text{P}}$, the saturation of the overshoot region starts to decrease slowly (see Fig. 4c), until a non-monotone profile with overshoot saturation $S \approx 0.631$ is reached. In general, the saturation approaches a value between S^* and $\min\{S^{\text{P}}, S^{\text{Wolge}}\}$. During the decrease in saturation, the plateau region undergoes drainage. As the drainage region advances, it approaches the imbibition front from behind. When the drainage region reaches the imbibition front, abrupt transitions to imbibition are unavoidable. These are clearly seen as front fluctuations in Fig. 4c. For a more realistic hysteresis model with continuous scanning curves, these front fluctuations are expected to be absent. The width of the overshoot region increases linearly with time, because the difference $c_{\text{im}}(S \approx 0.631) - c_{\text{dr}}(S \approx 0.631) > 0$ is constant.

6.4 Problem d)

Solutions of Problem d) show the behaviour typical for Region I in the $(S^{\text{P}}, t^{\text{P}})$ -plane. The drainage front is faster than the imbibition front, and the solution finally approaches a monotone shock profile without overshoot.

Figure 4d shows that the temporal change of the solution for $t > t^{\text{P}}$ can be split into three phases. During the first phase, until $t \approx 250$ s, the numerical solution is stable and shows the expected decrease in the overshoot width at the rate $48 \mu\text{m/s}$. Next, for $t > 250$ s, the overshoot saturation starts to decrease and abrupt fluctuations due to the discontinuous change between drainage and imbibition occur as observed in Region III. In the final phase, for $t > 450$ s, a simple monotone shock profile propagates with the expected dimensionless velocity of $c_{\text{im}}(S^{\text{in}}) = 1.338$ corresponding to 0.00352 cm/s .

6.5 Problem e)

Problem e) illustrates the importance of the time parameter t^{P} for the propagation of overshoot solutions. When t^{P} is too small, the initial overshoot region is too narrow. Capillary smoothing of the drainage front approaches the imbibition front from behind. This results in a decay of the overshoot. Because the decay implies abrupt changes between drainage and imbibition at the leading front, abrupt fluctuations again appear as in Regions I and III.

The numerical solution of problem e) is shown in Fig. 4e. It is typical for parameters in Region IV of the $(S^{\text{P}}, t^{\text{P}})$ -plane. As for Problem d), the long-time solution for $t \rightarrow \infty$ is a simple shock of height $S^{\text{in}} = 0.35$ moving at the identical speed $c_{\text{im}}(S^{\text{in}}) = 1.338$.

To facilitate the comparison of Fig. 4e where t is restricted to $0 \leq t \leq 250$ s with the other subfigures, the time interval $0 \leq t \leq 250$ s is shown in darker shade in Fig. 4b.

6.6 Influence of Hysteresis on Overshoot Propagation

All numerical simulations show that overshoot propagation and growth depend critically on hysteresis in the relative permeabilities, but not on hysteresis in capillary pressures. Setting $k_{\text{wim}}^r(S) = k_{\text{odr}}^r(S)$, but keeping $P_{\text{cim}}(S) \neq P_{\text{cdr}}(S)$, for given time-dependent boundary conditions, the leading imbibition front is slower than the trailing drainage front. As a result, the width of the overshoot shrinks until a monotone saturation profile is left (similar to Region I shown in Subfigure d) of Fig. 4). On the other hand for $k_{\text{wim}}^r(S) \neq k_{\text{odr}}^r(S)$, propagation and growth are both observed independently of whether there is hysteresis in $P_c(S)$ or $D(S)$. This was checked extensively. The same conclusion follows from a graphical analysis of the fractional flow functions as in Sect. 4.

7 Summary

Contrary to widespread belief and expectations, the present article finds an abundance of strongly pronounced saturation overshoot profiles as solutions to the standard two-phase flow equations with hysteresis in the relative permeabilities. Note that hysteresis of capillary pressures is not required for saturation overshoot. Hysteresis in capillary pressures enters as $D_{\text{im}} \neq D_{\text{dr}}$ and causes a difference in steepness or smearing between the leading imbibition and the trailing drainage front.

The height of the overshoot depends sensitively on the model parameters and the initial data. It can be much more pronounced than the shallow saturation overshoot first documented in Hilfer and Steinle (2014). As in Hilfer and Steinle (2014) it is emphasized here again, that constant Q and constant S^{in} are assumed for the boundary conditions at the left boundary. This differs from those experiments, where the flux of the wetting phase and the pressure of the non-wetting phase are controlled at the boundary.

The subset of initial conditions consisting of step functions has been systematically explored by means of generating the initial step functions through a time-varying boundary condition. Four different parameter regimes comprising travelling and non-travelling overshoot profiles were found. Increasing and decreasing width and height of the overshoot region are possible. The solutions can generally be predicted up to capillary smoothing effect from the fractional flow functions of the model. The highly idealized jump-type hysteresis can lead to abrupt saturation changes when the displacement process switches between drainage and imbibition. Nevertheless, the results are physically plausible and believed to be representative also for more realistic hysteresis models with continuous scanning curves. The systematic exploration of the initial conditions is the first indispensable step towards a full understanding of saturation overshoot.

Acknowledgments The authors acknowledge financial support from the Deutsche Forschungsgemeinschaft.

References

- Alt, H., Luckhaus, S., Visintin, A.: On nonstationary flow through porous media. *Ann. Mat. Pura Appl.* **136**, 303 (1984)
- Alt, H., Luckhaus, S.: Quasilinear elliptic-parabolic differential equations. *Math. Z.* **183**, 311 (1983)
- Beliaev, A., Hassanizadeh, S.: A theoretical model of hysteresis and dynamic effects in the capillary relation for two-phase flow in porous media. *Transp. Porous Media* **43**, 487 (2001)

- Cueto-Felgueroso, L., Juanes, R.: Nonlocal interface dynamics and pattern formation in gravity-driven unsaturated flow through porous media. *Phys. Rev. Lett.* **101**, 244504 (2008)
- Cueto-Felgueroso, L., Juanes, R.: Stability analysis of a phase-field model of gravity-driven unsaturated flow through porous media. *Phys. Rev. E* **79**, 036301 (2009)
- di Carlo, D.: Stability of gravity-driven multiphase flow in porous media: 40 years of advancements. *Water Resour. Res.* **49**, 4531 (2013)
- Duijn, C., Peletier, L., Pop, I.: A new class of entropy solutions of the Buckley–Leverett equation. *SIAM J. Math. Anal.* **39**, 507 (2007)
- Duijn, C., Fan, Y., Peletier, L., Pop, I.: Travelling wave solutions for degenerate pseudo-parabolic equations modelling two-phase flow in porous media. *Nonlinear Anal. Real World Appl.* **14**, 1361 (2013)
- Egorov, A., Dautov, R., Nieber, J., Sheshukov, A.: Stability analysis of gravity-driven infiltrating flow. *Water Resour. Res.* **39**, 1266 (2003)
- Eliassi, M., Glass, R.: On the porous-continuum modeling of gravity-driven fingers in unsaturated materials: extension of standard theory with a hold-back-pile-up effect. *Water Resour. Res.* **38**, 1234 (2002)
- Hilfer, R.: Macroscopic capillarity and hysteresis for flow in porous media. *Phys. Rev. E* **73**, 016307 (2006)
- Hilfer, R.: Macroscopic capillarity without a constitutive capillary pressure function. *Phys. A* **371**, 209 (2006)
- Hilfer, R., Steinle, R.: Saturation overshoot and hysteresis for twophase flow in porous media. *Eur. Phys. J. Spec. Top.* **223**, 2323 (2014)
- Otto, F.: L 1-contraction and uniqueness for quasilinear elliptic-parabolic equations. *J. Differ. Equ.* **131**, 20 (1996)
- Rätz, A., Schweizer, B., Angew. Z.: Hysteresis models and gravity fingering in porous media. *Math. Mech.* **94**, 645 (2014)
- Xiong, Y.: Flow of water in porous media with saturation overshoot: a review. *J. Hydrol.* **510**, 353 (2014)